Effect of Tension and Compression Stress on the Magnetic Losses in a Low-Carbon Steel

Abderraouf Ouazib, Mathieu Domenjoud, Patrick Fagan, and Laurent Daniel

Université Paris-Saclay, CentraleSupélec, CNRS, Laboratoire de Génie Electrique et Electronique de Paris, 91192 Gif-sur-Yvette, France
Sorbonne Université, CNRS, Laboratoire de Génie Electrique et Electronique de Paris, 75252 Paris, France

This work is an experimental study of the evolution of magnetic losses in dc-04 steel under static mechanical stress. The material was subjected, in the elastic regime, to uniaxial stress at levels from −90 to 90 MPa, and the evolution of magnetic losses, from quasi-static regime to 300 Hz (under controlled sinusoidal magnetic induction), was monitored. The analysis of the experimental results (remanent induction, coercive field, different components of losses) shows the non-trivial dependency of the stress-loss relationship to frequency. A loss separation analysis was performed to interpret the results. Considering the skin effect and its evolution with stress, hysteresis, eddy current, and anomalous losses are analyzed. The observed variations with frequency are then attributed to the change in the balance between the different components of losses, each showing a different sensitivity to stress depending on frequency. The study provides a phenomenological description of the frequency-dependent loss behavior of magnetic materials under tensile and compressive mechanical stress.

***Index Terms*— Ferromagnetic materials, iterative learning control, magnetic hysteresis, magnetic loss separation, magneto-mechanical effects.**

I. Introduction

MAGNETIC losses are a key factor in the design and optimization of electrical machines [1], [2], [3]. Previous works addressed the effect of stress on magnetic losses, mostly for tensile loadings, but sometimes including the effect of compressive stress [4], [5], [6], [7], or more rarely the effect of multiaxial stress [8], [9]. These works are usually restricted to a single excitation frequency and they are dedicated to electrical steel sheets, with low thickness, allowing to neglect skin effect, but limiting the compression stress to low levels (to prevent bulking). In the present work, the use of thick samples allowed us to explore the effect of high levels of compressive and tensile stresses on the magnetic losses of a dc-04 steel at different frequencies.

After introducing the experimental setup and waveform-control algorithm, $B(H)$ hysteresis loops, anhysteretic curves, measured remanent induction B_r and coercive field H_c are shown. The evolution of magnetic losses as a function of frequency, stress, and maximum field amplitude is then discussed. The stress–sensitivity of the skin effect is considered in the analysis of stress-dependent magnetic losses.

II. Experimental Setup

The experimental setup (Fig. 1, [10], [11]) is designed to apply simultaneously magnetic field H and uniaxial stress σ parallel to the applied magnetic field H on magnetic samples. The studied sample is 250 × 20 × 2 mm dc-04 steel. The magnetic arrangement consists of a pair of U-shaped Fe-Si yokes, ensuring the closure of the magnetic flux. Power is supplied to an excitation coil around the sample by a Kepco 72-14MG amplifier. A Teslameter (FM302) and a transverse Hall probe (20 mT AS-VTP) are employed to measure the magnetic field (in the measurement area). The induced voltage from a B-coil (50 turns) wound around the sample is time-integrated to determine the induction B through the sample. A constant stress is applied via a Zwick/Roell Z030 tension-compression machine. A DS 1006 dSPACE processor ensures the acquisition and control of signals, operating at a sampling frequency of 50 kHz. More details about the experimental setup, associated levels of noise, and measurement accuracy can be found in [10] and [11].

An iterative learning control algorithm was implemented to ensure a sinusoidal voltage in the B-coil [12], [13]. The form factor error and total harmonic distortion of the resulting signal did not exceed 0.5% and 0.12%, respectively. The errors in maximum induction B_{max} did not exceed 1%.

III. $B(H)$ Loops, Anhysteretic Measurements, and Magnetic Losses

Hysteresis loops, reaching a maximum induction value $B_{max} = 1.7$ T close to saturation, and corresponding anhysteretic measurements under static uniaxial stress σ levels from −90 to 90 MPa are shown in Fig. 2. The quasi-static frequency was identified as 1 Hz: the losses did not change when reducing the frequency further. As detailed in [11] and [14], the magnetic response of this low-carbon steel is very sensitive to applied stress. The non-monotonicity of the effect of tensile stress can be observed: at a low magnetic field, tensile stresses up to 45 MPa increase the induction but further increase of stress decreases the induction.

Manuscript received 24 March 2024; revised 15 May 2024; accepted 19 May 2024. Date of publication 22 May 2024; date of current version 27 August 2024. Corresponding author: A. Ouazib (e-mail: abderraouf.ouazib@centralesupelec.fr).

Color versions of one or more figures in this article are available at https://doi.org/10.1109/TMAG.2024.3403968.

Digital Object Identifier 10.1109/TMAG.2024.3403968

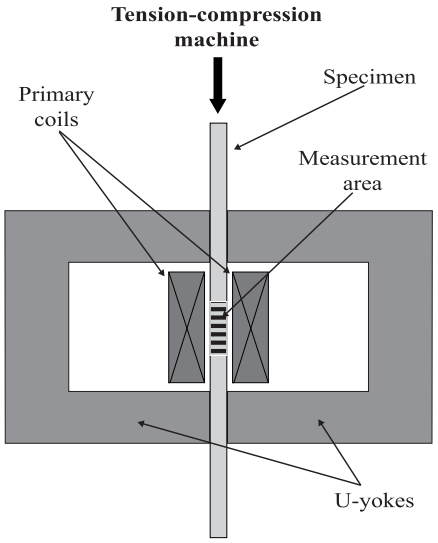

Fig. 1. Magneto-mechanical characterization setup [10], [11].

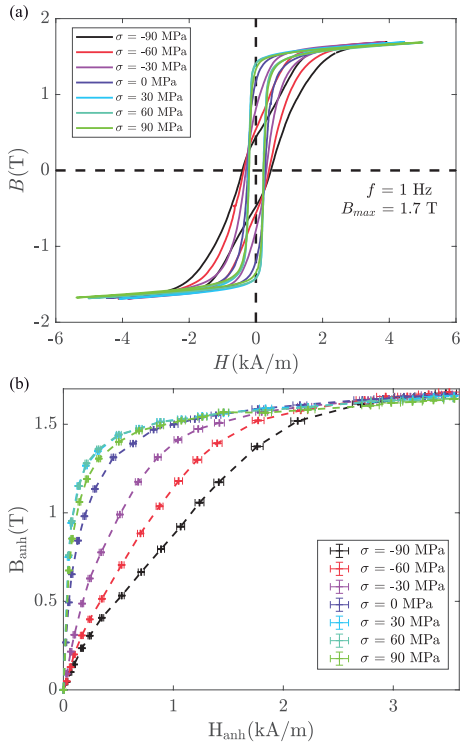

Fig. 2. (a) Quasi-static hysteresis loops and (b) anhysteretic measurements of magnetic induction B as a function of the applied magnetic field H for several levels of applied uniaxial stress σ. The dashed lines in the bottom figure are guides for the eye.

Hysteretic magnetic loops are then measured for the same levels of applied stress at frequencies f between 1 and 300 Hz, and for five values of maximum magnetic induction between 0.5 and 1.7 T. The stress levels are chosen to remain below, but close to the yield stress of the sample (about 120 MPa [11]) and below the Euler buckling critical compressive load (corresponding to about −300 MPa here). Typical results are shown in Fig. 3.

The sensitivity to stress appears to be strongly connected to the frequency. To investigate this effect, remanent induction B_r and coercive field H_c are extracted from hysteresis loops.

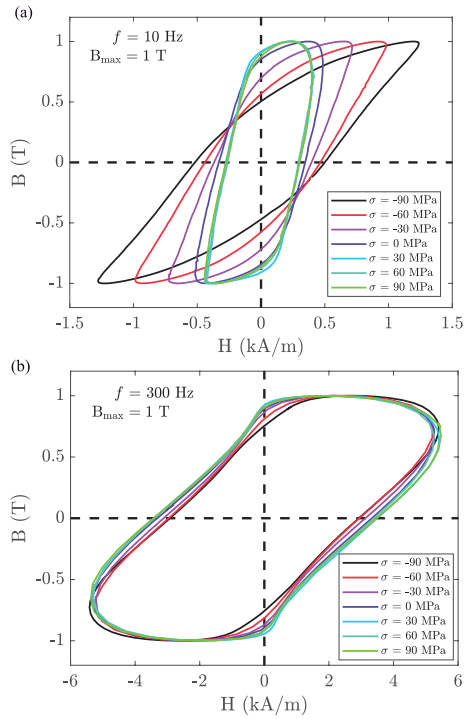

Fig. 3. Measured magnetic induction B as a function of the applied magnetic field H for B_{max} = 1 T at (a) 10 Hz and (b) 300 Hz for several levels of applied uniaxial stress σ.

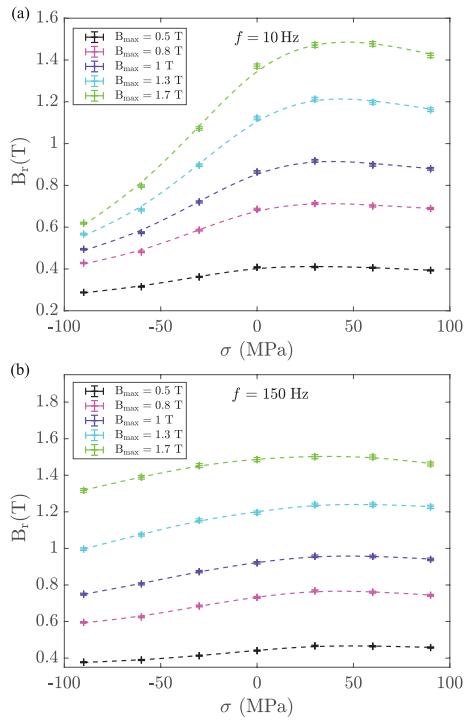

Fig. 4. Remanent magnetic induction B_r at (a) 10 Hz and (b) 150 Hz as a function of the applied uniaxial stress σ for several levels of maximum induction B_{max}. The dashed lines are guides for the eye.

The results are shown in Figs. 4 and 5, for $B_{max} = 1$ T, and for frequency values of 10 and 150 Hz, as a function of the applied uniaxial stress.

Regarding the remanent induction B_r (Fig. 4), a difference of +96% and +25% between −90 and 90 MPa is found at 10 and 150 Hz, respectively. Whatever the frequency, the

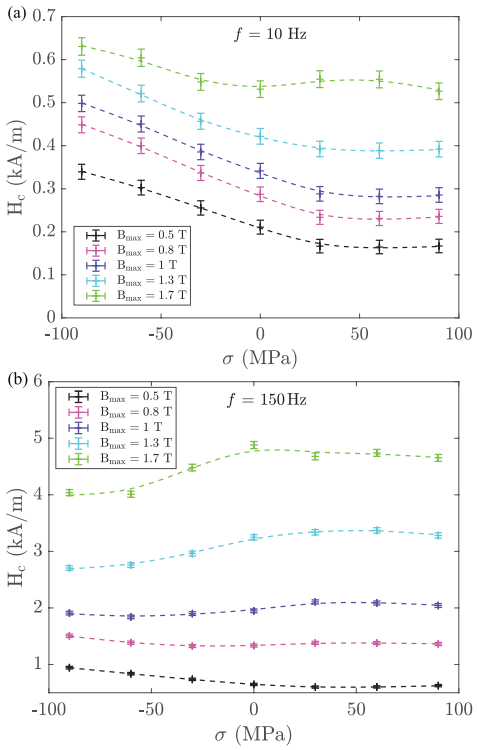

Fig. 5. Coercive field H_c at (a) 10 Hz and (b) 150 Hz as a function of the applied uniaxial stress σ for several levels of maximum induction B_{max}. The dashed lines are guides for the eye.

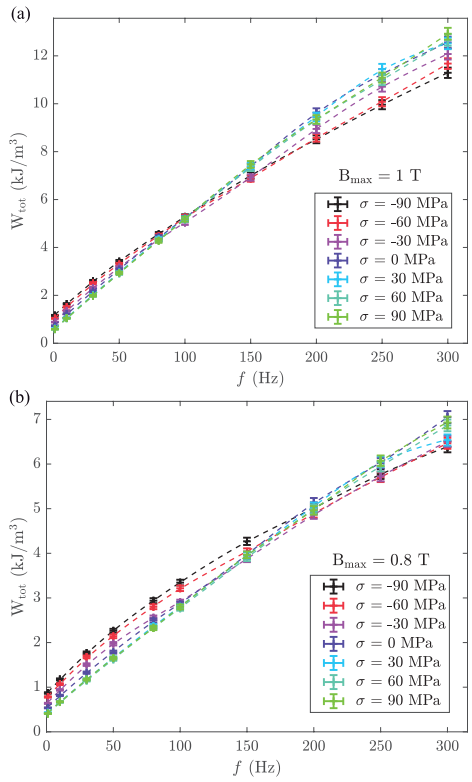

Fig. 6. Measured magnetic losses as a function of frequency f, for (a) B_{max} = 1 T and (b) 0.8 T, for different stress levels σ. The dashed lines are guides for the eye.

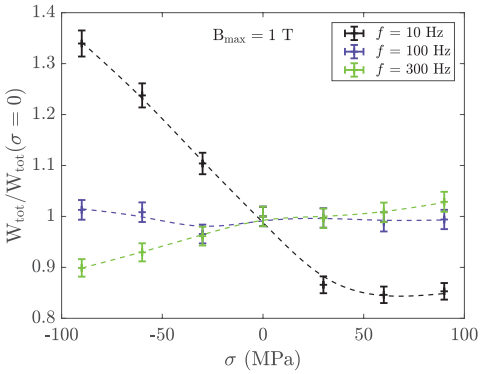

Fig. 7. Measured magnetic losses at 10, 100, and 300 Hz as a function of the applied uniaxial stress σ for a maximum induction B_{max} = 1 T. For each frequency, W_{tot} is normalized by its value under no applied stress. The dashed lines are guides for the eye. At 10 Hz (resp. 300 Hz), magnetic losses decrease (resp. increase) with stress. At 100 Hz, the magnetic losses are almost insensitive to stress.

maximum value of B_r is found close to +40 MPa. This evolution, observed for all maximum induction B_{max}, is connected to the non-monotonic evolution of the magnetic permeability observed and discussed in Fig. 2.

Regarding the coercive field H_c (Fig. 5), a −42% (resp. +10%) difference is found between −90 and 90 MPa at 10 Hz (resp. 150 Hz). At low frequencies, the coercive field H_c increases with the applied stress. At high frequency, it decreases with the applied stress. The frequency at which the trend reverses is a function of the applied maximum induction B_{max}. For B_{max} equal to 0.8 T, for instance, the reversal appears for a frequency close to 150 Hz.

To analyze the effect of stress and frequency on magnetic losses, the area of each hysteresis loop is evaluated, providing the total magnetic losses W_{tot} in the sample. The error bars represented for losses on the graph are estimated based on the errors estimated on the magnetic induction B and the magnetic field H adding the errors from the control process of the sine wave. Details about the error calculation for the magnetic induction and the magnetic field can be found in [10]. These errors were added to the accuracy errors estimated from the P-ILC algorithm.

Fig. 6 shows the results obtained for B_{max} equal to 1 and 0.8 T. As expected, magnetic losses monotonically increase with the frequency at all stress levels. However, at low frequencies, whatever the level of B_{max}, compression increases the magnetic losses. The effect is the opposite at high frequency. The frequency for which the sensitivity to stress vanishes is close to 100 Hz for B_{max} = 1 T and close to 200 Hz for B_{max} = 0.8 T. The plot of the total magnetic losses—normalized by the losses under no applied stress—as a function of stress (Fig. 7) confirms this complex behavior: depending on the frequency, the application of stress can either increase or decrease the level of total magnetic losses W_{tot}. A loss separation approach is conducted in Section IV to analyze this stress dependence of magnetic losses further.

IV. Loss Separation

The total magnetic losses W_{tot} are divided into three components

$$W_{tot} = W_{hyst} + W_{class} + W_{exc}. \quad (1)$$

Hysteresis losses W_{hyst} are related to the magnetic domain walls' motion under an external magnetic field. They are

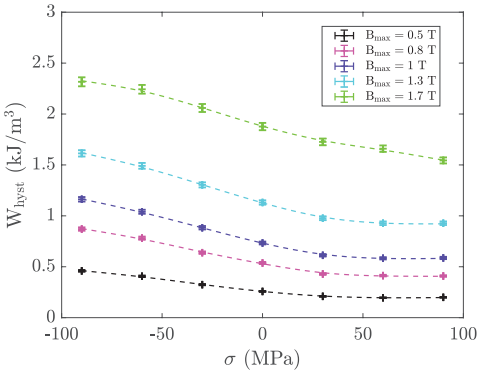

Fig. 8. Measured magnetic hysteresis losses (at 1 Hz) as a function of the applied uniaxial stress σ. The dashed lines are guides for the eye.

independent of the frequency and are equal to the total losses in the quasi-static regime [$W_{hyst} = W_{tot}(f \approx 0)$]. Hysteresis losses can be extracted from the measurements at $f = 1$ Hz [see Fig. 2(a)]. Fig. 8 shows the evolution of hysteresis losses W_{hyst} as a function of σ for various levels of B_{max}. A decrease of W_{hyst} with stress is observed with progressive stabilization under tension. These results are consistent with previous observations [4], [9].

Classical losses W_{class} are connected to the macroscopic eddy current in the material. They can be obtained from the resolution of Maxwell equations [15] and are usually written as follows:

$$W_{class} = \frac{\pi^2}{6} \lambda d^2 B_{max}^2 f \tag{2}$$

where λ is the conductivity of the material, usually considered insensitive to stress [16] ($\lambda = 7.0\ 10^6$ S·m^{-1} for dc-04), d is the thickness of the sample ($d = 2$ mm here). This expression is commonly used to separate magnetic losses [4], [5], [9], [17] when the dimensions of the sample allow neglecting the skin effect. In the configuration of a thick sample, the skin effect is significant and cannot be neglected (see appendix A). A generalized formulation of classical losses, taking into account skin effect [15], can then be employed

$$W_{class} = \frac{\pi}{2} \frac{\gamma B_{max}^2}{\mu} \frac{\sinh(\gamma) - \sin(\gamma)}{\cosh(\gamma) - \cos(\gamma)} \tag{3}$$

with

$$\gamma = \sqrt{\pi \lambda \mu d^2 f} \tag{4}$$

where μ is the magnetic permeability of the material. Due to the nonlinearity of the behavior, μ is a function of stress and induction. It can be extracted from the anhysteretic curves [see Fig. 2(b)]

$$\mu(B_{max}, \sigma) := \mu_{anh}(B_{anh}, \sigma) = \left(\frac{B_{anh}}{H_{anh}}\right)_{\sigma}. \tag{5}$$

Based on this definition of the classical losses, the evolution of W_{class} as a function of frequency and stress for a maximum induction B_{max} of 1 T is shown in Fig. 9. Classical losses increase with frequency whatever the stress level and decrease with the applied stress whatever the frequency.

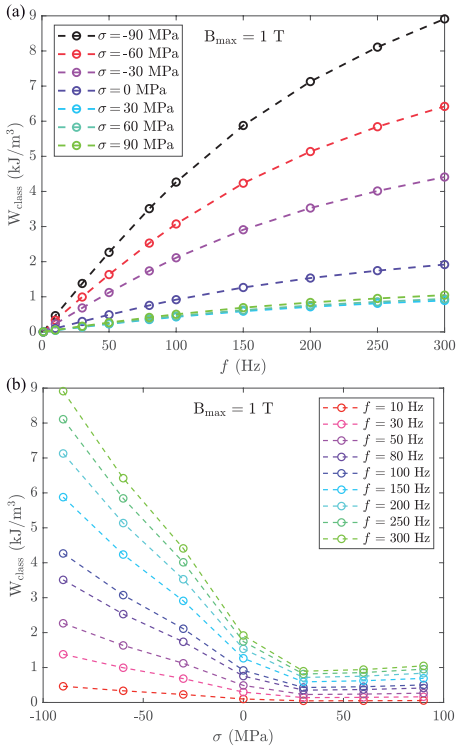

Fig. 9. Magnetic classical losses for B_{max} = 1 T (a) function of frequency for several levels of applied uniaxial stress σ and (b) function of σ for different frequencies f. The dashed lines are guides for the eye.

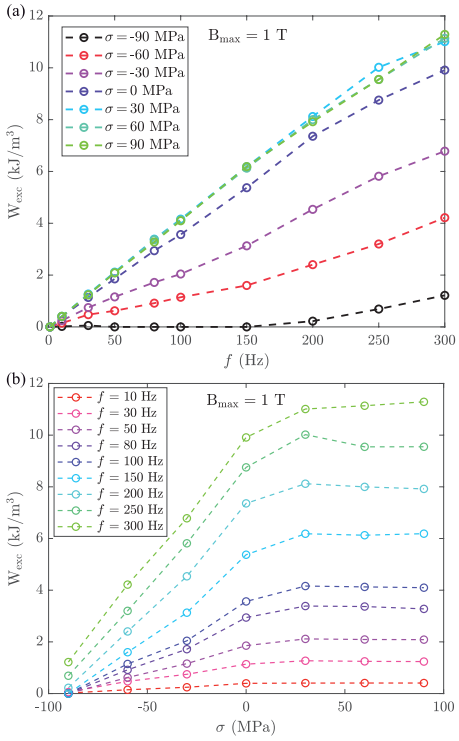

Fig. 10. Magnetic excess losses for B_{max} = 1 T (a) function of frequency f for several levels of applied uniaxial stress σ and (b) function of σ for different frequencies. The dashed lines are guides for the eye.

Excess losses W_{exc} are obtained by the difference between the total losses and the hysteresis and classical components

$$W_{exc} = W_{tot} - \left(W_{hyst} + W_{class}\right). \tag{6}$$

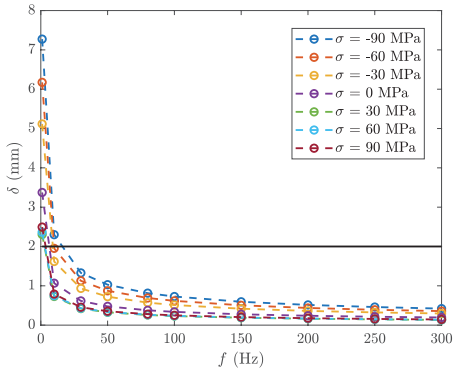

Fig. 11. Skin depth δ from 1 to 300 Hz, for several levels of applied uniaxial stress σ.

Calculated excess losses are shown in Fig. 10, as a function of frequency [Fig. 10(a)] and applied stress [Fig. 10(b)]. At a given frequency, W_{exc} increases with applied stress and, at a given applied stress, increases with frequency.

This loss separation approach explains the complex trends observed for the evolution of magnetic losses under applied stress for dc-04. At low frequencies, hysteresis and classical losses dominate so the total losses tend to decrease with stress. As frequency increases, excess losses become more and more significant, leading to a reversal of this trend and an increase in total losses with stress at high frequency.

V. Conclusion

This article is an experimental study on the magneto-elastic behavior of low-carbon steel. Hysteresis loops, magnetic losses, coercive field, and remanent induction were collected at various levels of tensile and compressive stress, various frequencies, and various maximum induction levels. Anhysteretic curves were also recorded. Taking the skin effect into account, a loss separation approach was implemented and allowed interpretation of the non-trivial evolution of the different magnetic loss components as a function of stress, frequency, and magnetic induction.

Appendix A
Skin Effect

The skin depth δ depends on material properties (electrical conductivity λ and magnetic permeability μ) and frequency f according to the standard formula [15]

$$\delta = \frac{1}{\sqrt{\pi \lambda \mu f}}. \tag{7}$$

The value for μ can be extracted from anhysteretic measurements (see Fig. 2) to evaluate its dependence on stress. Fig. 11 plots the stress dependence of the skin depth δ for dc-04. Given the thickness of the sample in the present study ($d = 2$ mm), the figure shows that the skin effect cannot be neglected even at low frequencies.

References

[1] D. Miyagi, N. Maeda, Y. Ozeki, K. Miki, and N. Takahashi, "Estimation of iron loss in motor core with shrink fitting using FEM analysis," *IEEE Trans. Magn.*, vol. 45, no. 3, pp. 1704–1707, Mar. 2009.

[2] L. Bernard and L. Daniel, "Effect of stress on magnetic hysteresis losses in a switched reluctance motor: Application to stator and rotor shrink fitting," *IEEE Trans. Magn.*, vol. 51, no. 9, pp. 1–13, Sep. 2015.

[3] K. Yamazaki, Y. Sato, M. Domenjoud, and L. Daniel, "Iron loss analysis of permanent-magnet machines by considering hysteresis loops affected by multi-axial stress," *IEEE Trans. Magn.*, vol. 56, no. 1, Jan. 2020, Art. no. 7503004.

[4] M. LoBue, C. Sasso, V. Basso, F. Fiorillo, and G. Bertotti, "Power losses and magnetization process in Fe–Si non-oriented steels under tensile and compressive stress," *J. Magn. Magn. Mater.*, vol. 215, pp. 124–126, Jun. 2000.

[5] V. Permiakov, L. Dupré, A. Pulnikov, and J. Melkebeek, "Loss separation and parameters for hysteresis modelling under compressive and tensile stresses," *J. Magn. Magn. Mater.*, vols. 272–276, pp. 553–554, May 2000.

[6] D. Singh, P. Rasilo, F. Martin, A. Belahcen, and A. Arkkio, "Effect of mechanical stress on excess loss of electrical steel sheets," *IEEE Trans. Magn.*, vol. 51, no. 11, Nov. 2015, Art. no. 1001204.

[7] J. Karthaus, S. Elfgen, N. Leuning, and K. Hameyer, "Iron loss components dependent on mechanical compressive and tensile stress in non-oriented electrical steel," *Int. J. Appl. Electromagn. Mech.*, vol. 59, no. 1, pp. 255–261, Mar. 2019.

[8] Y. Kai, Y. Tsuchida, T. Todaka, and M. Enokizono, "Influence of stress on vector magnetic property under alternating magnetic flux conditions," *IEEE Trans. Magn.*, vol. 47, no. 10, pp. 4344–4347, Oct. 2011.

[9] U. Aydin et al., "Effect of multi-axial stress on iron losses of electrical steel sheets," *J. Magn. Magn. Mater.*, vol. 469, pp. 19–27, Jan. 2019.

[10] M. Domenjoud, E. Berthelot, N. Galopin, R. Corcolle, Y. Bernard, and L. Daniel, "Characterization of giant magnetostrictive materials under static stress: Influence of loading boundary conditions," *Smart Mater. Struct.*, vol. 28, no. 9, Sep. 2019, Art. no. 095012.

[11] M. Domenjoud and L. Daniel, "Effects of plastic strain and reloading stress on the magneto-mechanical behavior of electrical steels: Experiments and modeling," *Mech. Mater.*, vol. 176, Jan. 2023, Art. no. 104510.

[12] S. Zurek, P. Marketos, T. Meydan, and A. J. Moses, "Use of novel adaptive digital feedback for magnetic measurements under controlled magnetizing conditions," *IEEE Trans. Magn.*, vol. 41, no. 11, pp. 4242–4249, Nov. 2005.

[13] P. Fagan et al., "Iterative methods for waveform control in magnetic measurement systems," *IEEE Trans. Instrum. Meas.*, vol. 71, 2022, Art. no. 6006113.

[14] L. G. D. Silva, A. Abderahmane, M. Domenjoud, L. Bernard, and L. Daniel, "An extension of the vector-play model to the case of magneto-elastic loadings," *IEEE Access*, vol. 10, pp. 126674–126686, 2022.

[15] G. Bertotti, *Hysteresis in Magnetism: For Physicists, Materials Scientists, and Engineers*. San Diego, CA, USA: Academic, 1998.

[16] F. Zhang, H. Li, C. Zhao, and R. Jia, "Effect model of stress and plastic deformation on conductivities of various magnetic materials," *IEEE Access*, vol. 8, pp. 82741–82746, 2020.

[17] F. J. G. Landgraf et al., "Loss decomposition in plastically deformed and partially annealed steel sheets," *J. Magn. Magn. Mater.*, vol. 502, May 2020, Art. no. 166452.